Compositional Optimization of Alloy Fe_xNi_y(OH)₂ Nanoparticles for Alkaline Electrochemical Oxygen Evolution

L.F. Greenlee^a, P. Acharya^a, Z. Nelson^a

^aRalph E. Martin Department of Chemical Engineering, University of Arkansas, Fayetteville, Arkansas 72701, USA

Alloy FeNi nanoparticles were synthesized and evaluated as electrocatalysts for the oxygen evolution reaction in alkaline electrolyte. Electron microscopy imaging indicates nanoparticles were formed with a spherical morphology, and initial elemental analysis suggests significant oxygen content in the bimetallic particles. A molar ratio range from 5:1 to 1:5 Fe:Ni in the asnanoparticles was tested. The synthesized effect polyvinylpyrrolidone stabilizer on nanoparticle performance was also evaluated. Catalytic performance of the nanoparticles increased with decreasing Fe:Ni molar ratio and PVP:Ni molar ratio. Alloy nanoparticles synthesized with a Fe:Ni ratio of 1:5 and a PVP:Ni ratio of 0.001 resulted in an overpotential of 295 mV at 10 mA/cm², a Tafel slope of 40 mV/dec, and a mass-based activity of 3343 mA/mg at 1.6 V vs. RHE.

Introduction

Electrolysis of water in alkaline conditions holds great promise as a cost-effective and environmentally-tractable method of producing hydrogen fuel (1, 2). However, the sluggish kinetics of the oxygen evolution reaction (OER) continue to limit the development and commercial implementation of electrolysis technology. In an alkaline environment, non-precious metal catalysts can be used, and much experimental research has pursued the development of active non-precious metal-based catalysts. Nickel hydroxide/oxide-based electrocatalysts have been well-studied as an active OER catalyst material (3-10), but recent findings have now pointed to the bimetallic iron-nickel combination in hydroxide or oxide form as perhaps the most active catalyst material for OER (11-18).

Louie, Bell and co-authors (19) recently demonstrated that intentional iron doping into a nickel hydroxide film causes significant enhancement in OER electrochemical performance. A subsequent study by Trotochaud, Boettcher and co-authors (12) demonstrated that unintentional iron doping into nickel hydroxide thin film catalysts occurs from ppm- to ppb-level iron impurities in alkaline electrolytes; the iron incorporates into the nickel hydroxide structure, and causes at least an order of magnitude increase in current density. Freibel et al. subsequently demonstrated that iron may in fact be the active site of OER, with nickel hydroxide acting as a host (11). The majority of the work performed thus far to investigate how iron content in an Fe_xNi_y(OH)₂ catalyst affects OER has been performed on thin film catalysts; Burke et al. specifically describe the need for catalyst architectures that reduce mass transport limitations and allow improved access to more active sites per unit mass of catalyst (1). As a result, there is an

interest in developing nanoscale catalysts that are composed of iron and nickel and result in greatly improved performance metrics for OER over their thin film counterparts.

Recently, in related research, our work has shown that a core-shell Fe_xNi_y(OH)₂ catalyst may be synthesized in nanoparticle form, resulting in significant increases in the mass activity of these catalysts for OER. However, these, and similar, nanoparticle catalysts remain unoptimized for OER, and it is unknown whether optimal performance will occur at similar Fe content as that identified in the thin films work of Trotochaud et al. (12). Other related work published recently reports on FeNi-based nanocatalysts (20-26) but an evaluation of the molar bimetallic ratio and the effect of key synthesis parameters such as the concentration of ligand stabilizers, remains largely uninvestigated (22). These recent publications point to exceptionally high mass activities for OER, demonstrating the importance of this class of OER catalyst materials and underscoring the need for further development of FeNi-based nanomaterial electrocatalysts. particular, the presence of ligand stabilizers such as polyvinylpyrrolidone (PVP) on the surface of synthesized nanoparticle catalysts has been implicated in the reduction of electrochemical performance (27, 28); however, conflicting evidence suggests that in some cases, and perhaps for specific catalytic reactions, the presence of a ligand such as PVP may actually enhance electrocatalytic activity (29). As many approaches to nanoparticle synthesis involve colloidal solution-phase chemistry and utilize stabilizing ligands, it is critical to understand the role of the ligand in catalytic performance. Further, based on the thin film (Fe_xNi_y(OH)₂) catalyst work of Trotochaud et al. (12), Friebel et al. (11), and Klaus et al. (13), it is clear that the amount of iron in an iron-nickel bimetallic hydroxide catalyst is a key parameter to control in the optimization of these catalysts for OER performance.

In this paper, we present results for the optimization of a FeNi-based ($Fe_xNi_y(OH)_2$) alloy nanoparticle catalyst. Nanoparticles were synthesized with a nominal alloy morphology, and the atomic ratio of iron to nickel was varied from 5:1 to 1:5. The influence of the stabilizer PVP on catalytic performance was also evaluated. Once synthesized, the nanoparticles were characterized via electron microscopy and evaluated for electrochemical performance in purified 1 M KOH. Electrochemical performance of this series of nanoparticle catalysts was evaluated via linear sweep voltammetry and cyclic voltammetry. Alloy nanoparticle performance is compared to the performance of a Fe@Ni core-shell nanoparticle catalyst.

Experimental

Materials

All chemicals used were ACS grade, unless otherwise specified. Iron sulfate heptahydrate (FeSO₄*7H₂O), nickel chloride hexahydrate (NiCl₂*6H₂O), sodium borohydride (NaBH₄), potassium hydroxide (KOH), and polyvinylpyrrolidone (MW = 40,000 g/mol) were purchased from a commercial supplier and used as received. The stabilizer aminotris(methylene phosphonic acid) (ATMP) was obtained as a laboratory sample from Dequest Italmatch Chemicals. Purified water was produced by a Millipore Milli-Q® Integral water purification system.

Nanoparticle Synthesis and Characterization

Alloy nanoparticles were synthesized via an aqueous-based solution phase reduction reaction method, as shown, generally, in Figure 1. First, the iron sulfate precursor is

combined with the stabilizer ATMP and purified water and mixed. Next, the nickel chloride precursor and PVP are combined in solution and mixed; the nickel chloride/PVP solution is then added to the iron/ATMP solution, and the solution is mixed in a threeneck borosilicate glass flask under argon for 15 min. Subsequently, dissolved sodium borohydride is added to the solution at a ratio of 2.2:1 (mol:mol) borohydride to metal. This ratio accounts for the molar requirement for complete metal reduction and also accounts for the side reaction between water molecules and borohydride (30, 31). Once the borohydride solution is added, the solution is mixed under vacuum for 15 min. Hydrogen gas is visibly evolved, and a decrease in bubbling signals the completion of the reaction. The synthesized nanoparticles are then separated from the remainder of the synthesis solution via centrifugation and are resuspended in methanol for storage. Alloy nanoparticles were synthesized for a range of molar ratios of iron to nickel (5:1 to 1:5 (mol:mol)). The ratio of the two metals in the nanoparticles is varied by changing the starting concentrations of the two metal precursors. The ratio of ATMP:Fe was 0.05 (mol:mol) for all nanoparticles reported herein. The ratio of PVP:Ni was varied for several nanoparticle materials to evaluate the effect of PVP on catalyst performance. The range of ratios tested for PVP:Ni was 0.001 - 0.005 (mol:mol). In this work, allow nanoparticles are compared to a 1:1 (mol:mol) iron-nickel (Fe@Ni) core-shell nanoparticle material (32). The Fe@Ni core-shell nanoparticles were synthesized similarly, as shown in Figure 1. For core-shell synthesis, the Fe:ATMP ratio was 0.05 (mol:mol) and the PVP:Ni ratio was 0.005 (mol:mol). All nanoparticles were synthesized at a concentration of 1 g/L as Fe, and nickel concentrations were calculated based off of this starting iron concentration. Monometallic nanoparticles can be similarly synthesized; electrochemical results for monometallic nanoparticles synthesized via the nanoparticle synthesis approach shown in Figure 1 can be found elsewhere (32).

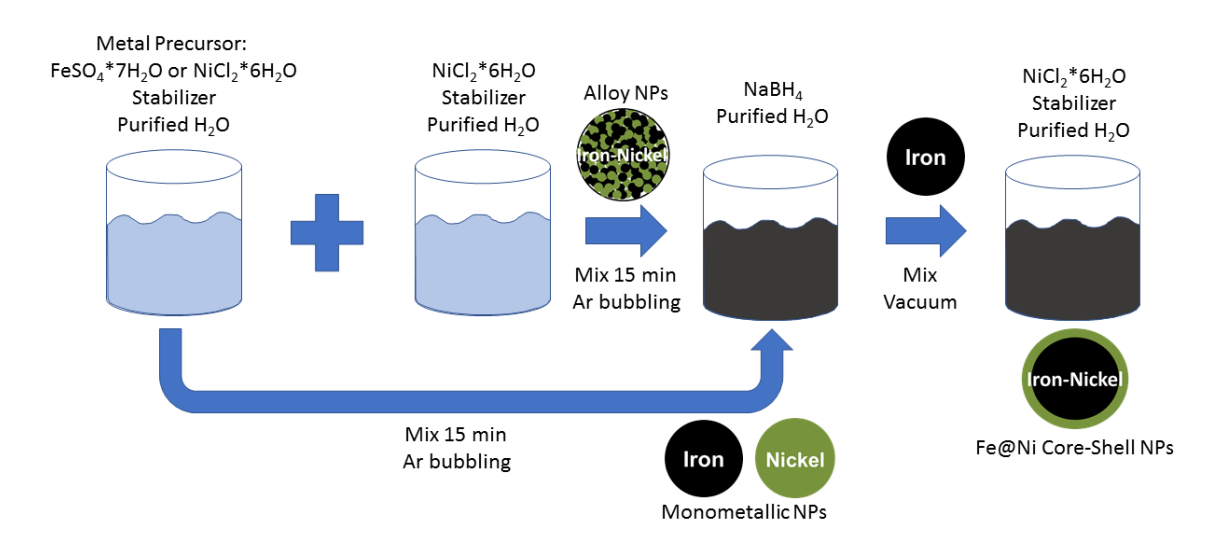


Figure 1. Schematic of general nanoparticle synthesis approach.

Nanoparticles were characterized via transmission electron microscopy (TEM) and energy dispersive x-ray spectroscopy (EDX) mapping. For TEM imaging, nanoparticles were suspended in methanol via sonication, diluted, and dropcast onto a lacey carbon copper grid (200 mesh).

Electrochemical Characterization

Electrochemistry experiments were performed on alloy nanoparticles and used 1 M KOH. For all experiments, the base electrolyte was purified via the approach established by Trotochaud et al. (12) and used in prior research in Candelaria et al. (32). Briefly, 1 M KOH solution is made with the commercial base and purified water. The solution is mixed with precipitated nickel hydroxide particles, mixed for several hours, and the nickel hydroxide precipitate is subsequently removed. This purification process is used to remove any iron impurities that are in the base electrolyte solution, as these impurities are known to incorporate into nickel hydroxide and change the electrochemical performance (12).

All electrochemistry experiments were performed in a stationary 3-electrode cell with a gold working electrode (surface area = $0.02~\rm cm^2$), a graphite rod counter electrode, and a silver/silver chloride (Ag/AgCl) reference electrode. The reference electrode was placed in a salt bridge containing 3.0 M sodium chloride (NaCl) to protect the reference electrode from degradation due to exposure to the base electrolyte. Synthesized nanoparticles were mixed in a methanol-based ink with an experimental ionomer developed for alkaline electrochemical environments (32) and dropcast onto the working electrode for a catalyst loading of 50 $\mu g/cm^2$. The ink was allowed to dry at room temperature and subsequently tested for OER performance. All measurements were compared to background measurements of the cleaned gold electrode. Linear sweep voltammetry and cyclic voltammetry techniques were used to evaluate the electrochemical performance of the nanoparticle catalysts. A Tafel analysis was performed on the linear region of the forward sweep obtained via cyclic voltammetry experiments. For all experiments, at least 20 cycles were measured and the cycles/sweeps reported are taken from the same cycle across samples.

Results and Discussion

Nanoparticle Morphology

Synthesized nanoparticles were imaged with TEM and representative images are shown in Figure 2 for alloy nanoparticles and ratios of 5:1, 1:1, and 1:5 Fe:Ni (mol:mol). All alloy nanoparticles had a roughly spherical shape and similar phase contrast in the bright field images. The nanoparticles appear agglomerated in the images taken and may also be agglomerated in the methanol-based nanoparticle inks prepared for electrochemistry. An ImageJ analysis of individual nanoparticles identified in these images suggests that the nanoparticles are typically less than 50 nm nominally, with sizes measured at 21 nm \pm 4 nm, 29 nm \pm 9 nm, and 15 nm \pm 4 nm for the 5:1, 1:1, and 1:5 Fe:Ni molar ratios, respectively. However, some nanoparticles may be larger than those measured, and the particle agglomeration prevents definitive size measurement. This initial analysis of the synthesized nanoparticles demonstrates successful formation of nanoparticulate materials, and all alloy catalysts synthesized for this work are expected to be nanoparticulate. Further imaging analysis at higher resolution, along with additional characterization, is needed for these materials to explore detailed morphology, structure, and composition and to delineate any differences beyond particle size between the different alloy compositions.

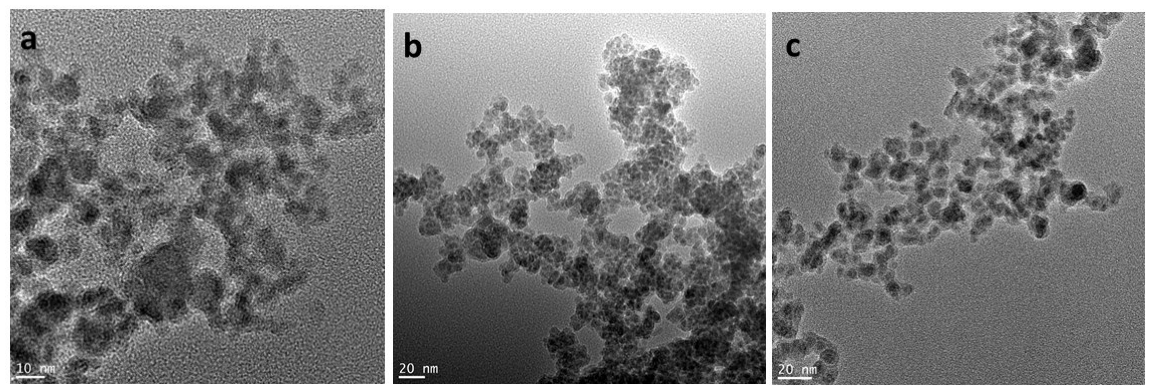


Figure 2. TEM images of iron-nickel alloy nanoparticles for Fe:Ni ratios of (a) 5:1, (b) 1:1, and (c) 1:5.

An initial set of high resolution TEM with EDX mapping analysis was performed for the 1:1 FeNi alloy nanoparticles and the 1:1 Fe@Ni core-shell nanoparticles (Figure 3), where a larger, isolated nanoparticle was analyzed for each sample. This data set demonstrates that the synthesis approach used in this work produces either alloy (i.e., homogeneously mixed bimetallic composition) or core-shell (i.e., iron core, nickel shell) morphologies in nanoparticle form. In the alloy nanoparticle analyzed in Figure 3a, the iron and nickel elemental maps suggest a visually homogenous distribution of the two elements across the entirety of the particle. In contrast, the iron and nickel elemental maps of Figure 3b suggest an iron core and a nickel shell. The iron map (shown in red) again appears relatively homogeneous across the visual area of the particle, while the nickel map (shown in yellow) suggests that there is less nickel through the core of the particle and more nickel concentrated at the outer shell. In addition to the information gained from the iron and nickel elemental maps, the oxygen elemental maps (shown in blue) suggest a significant oxygen content for both alloy and core-shell nanoparticles. The density difference of the pixilation between the two oxygen maps (alloy vs. coreshell) suggests that the alloy nanoparticle may have had more oxygen content than the core-shell nanoparticle. Further, the oxygen map of the core-shell nanoparticle in Figure 3b suggests that the oxygen content of the core-shell nanoparticle is located primarily in the shell of the nanoparticle. The presence of oxygen in the shell suggests that these nanoparticles are likely to be in oxide/hydroxide form; once exposed to alkaline electrolyte, it is likely that these nanoparticles would contain hydroxides at surfaces exposed to the electrolyte (12). Additional analysis and characterization of the 1:1 Fe@Ni core-shell nanoparticle catalyst of Figure 3b can be found elsewhere (32). A more detailed characterization analysis of the alloy nanoparticles will be the focus of future work.

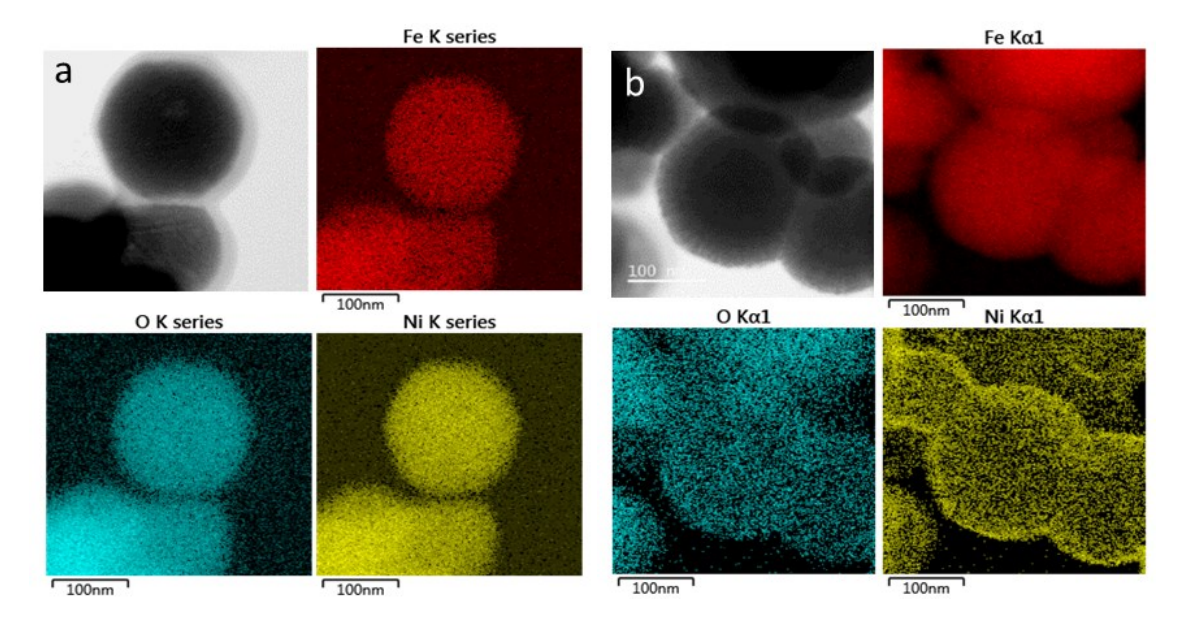


Figure 3. TEM images and EDX mapping: representative results for (a) 1:1 iron-nickel alloy nanoparticles and (b) 1:1 iron-nickel core-shell nanoparticles.

Electrochemical Performance

An electrochemical analysis of three sets of alloy nanoparticle catalysts is shown in Figure 4 for varying ratios of PVP:Ni and Fe:Ni. For this analysis, all nanoparticles were analyzed via linear sweep voltammetry, and Fe:Ni ratios of 5:1, 1:1, and 1:5 were evaluated. A range of PVP:Ni molar ratios of 0.001 - 0.005 was tested, where the PVP is used as a stabilizer during alloy nanoparticle synthesis. The PVP polymer molecules are combined with the nickel precursor in solution and provide colloidal stability to the suspension as the nanoparticles form. During nanoparticle growth, some of the PVP molecules adsorb onto the nanoparticle surface, and the resulting catalyst particles are expected to have a surface coating of stabilizer even after rinsing with methanol (30, 31).

The results shown in Figure 4 suggest that the PVP concentration used during synthesis may play a role in the electrocatalytic performance of these alloy nanoparticles, but the impact of PVP concentration may vary depending on the PVP concentration and the alloy nanoparticle bimetallic composition. Results for a molar ratio of 5:1 Fe:Ni and two alloy nanoparticle catalyst samples, each synthesized with a PVP:Ni ratio of 0.005 resulted in similar electrocatalytic performance (Figure 4a). In comparison, alloy nanoparticles tested at a ratio of 1:1 Fe:Ni for two different PVP:Ni ratios (0.002 and 0.005) suggest that the higher PVP:Ni ratio did not negatively impact OER performance, and may have resulted in a slight improvement in performance. In contrast, the 1:5 Fe:Ni alloy nanoparticles tested in Figure 3c resulted in a significant difference in catalytic performance for the two ratios of PVP:Ni tested (0.001 and 0.005). In this set of results, the decrease in the PVP:Ni ratio resulted in an increase in the overall current density measured, as well as an improvement in the overpotential (295 mV vs. 313 mV @ 10 mA/cm^2 for PVP:Ni = 0.001 vs. PVP:Ni = 0.005). These initial results suggest a potentially important role for PVP in the catalytic performance of these nanoparticles, and future work will involve evaluating a range of PVP:Ni ratios across the bimetallic

compositional space. Also of note in these results is the significant difference in catalytic performance observed as a function of Fe:Ni ratio.

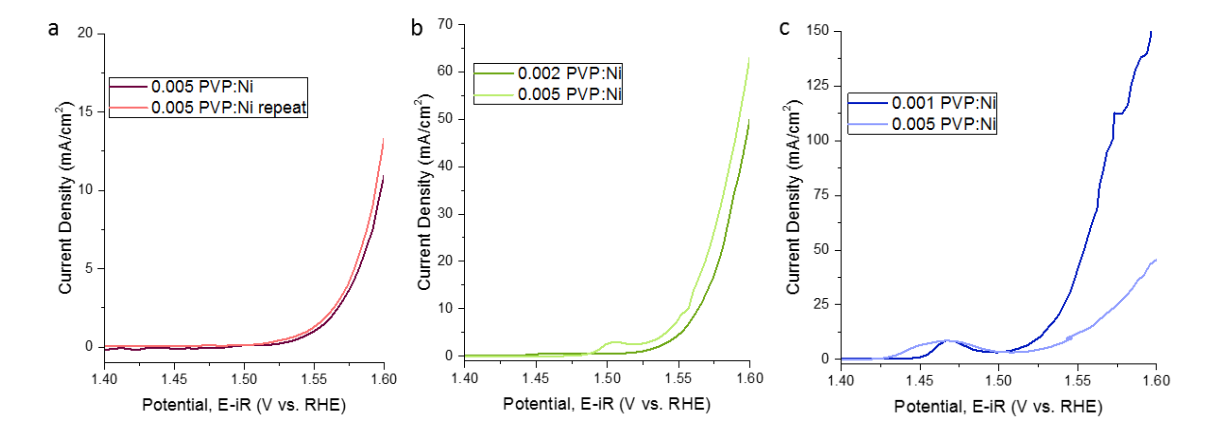


Figure 4. Effect of PVP:Ni ratio on the OER electrochemical performance of nanoparticles for alloy compositions of (a) 5:1 Fe:Ni, (b) 1:1 Fe:Ni, and (c) 1:5 Fe:Ni.

To further explore the role of Fe:Ni molar ratio in controlling the electrochemical activity of the alloy nanoparticle catalysts for OER, a range of ratios between 5:1 and 1:5 Fe:Ni was evaluated (Figure 5). Results for the alloy compositions are compared to the performance of a 1:1 Fe@Ni core-shell nanoparticle catalyst (32). Generally, as the ratio of iron to nickel decreased from 5:1 to 1:5 in the alloy nanoparticles, the performance of the nanoparticles improved; the measured current density increased as the iron content decreased, and the OER curves generally shifted to the left, with a decrease in the measured overpotential from 368 mV to 295 mV @ 10 mA/cm². In the data presented in Figure 5, the alloy nanoparticles were synthesized with a range of PVP:Ni ratios (0.001 – 0.005). Of note, the best performing nanoparticle catalyst had both the lowest tested ratio of Fe:Ni (1:5) and the lowest tested ratio of PVP:Ni (0.001). Except for the Fe:Ni ratios of 5:1 and 5:2, all ratios tested were synthesized with lower PVP:Ni ratios of 0.001 – 0.002. The nanoparticles with a 5:1 Fe:Ni ratio had a PVP:Ni ratio of 0.005, and the nanoparticles with a 5:2 Fe:Ni ratio had a PVP:Ni ratio of 0.003. The PVP:Ni and Fe:Ni ratios tested are summarized in Table 1, along with performance data for all nanoparticles tested. While further analysis is needed to delineate the effect of the PVP:Ni ratio on nanoparticle performance, it is clear from these results that the ratio of iron to nickel in these bimetallic alloy nanoparticles has a significant impact on the electrocatalytic performance for OER.

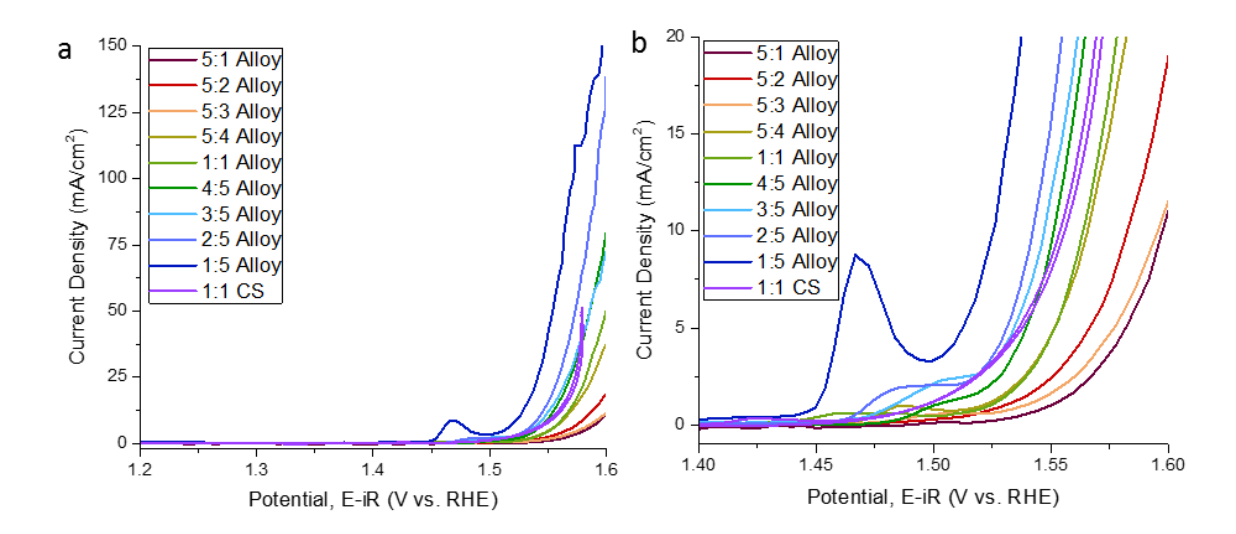


Figure 5. Nanoparticle catalyst electrochemical performance for alloy nanoparticles as a function of Fe:Ni (mol:mol) ratio. All ratios are reported in the legend as iron to nickel. Alloy nanoparticles are compared to a 1:1 Fe@Ni core-shell (CS) nanoparticle catalyst (32). (a) Current density production as a function of nanoparticle morphology and Fe:Ni ratio. (b) Current density data shown for a potential range of 1.4 - 1.6 V.

Nanoparticle catalytic performance is summarized in Figure 6, where current production is normalized to the mass of catalyst tested. The catalytic performance results, when normalized to geometric surface area (Figure 5), are quite similar to results previously reported for bimetallic FeNi thin films (11-13, 19). However, when normalized on a per mass basis, the current densities for the best-performing catalysts are several orders of magnitude greater than those reported for similar bimetallic thin films (12, 19). These results illustrate the benefits of developing a nanoparticulate-based OER catalyst, where the surface area to mass ratio is much lower and the mass transport limitations on the catalytic reactions are lowered, resulting in significant increases in mass-normalized catalytic activity. Further, in comparison to the 1:1 Fe@Ni core-shell nanoparticle catalyst, the performance of the 1:5 Fe:Ni alloy nanoparticle catalyst performed similarly. These results suggest that further compositional optimization of both the alloy and core-shell nanoparticle catalyst materials would likely result in improvements to OER performance.

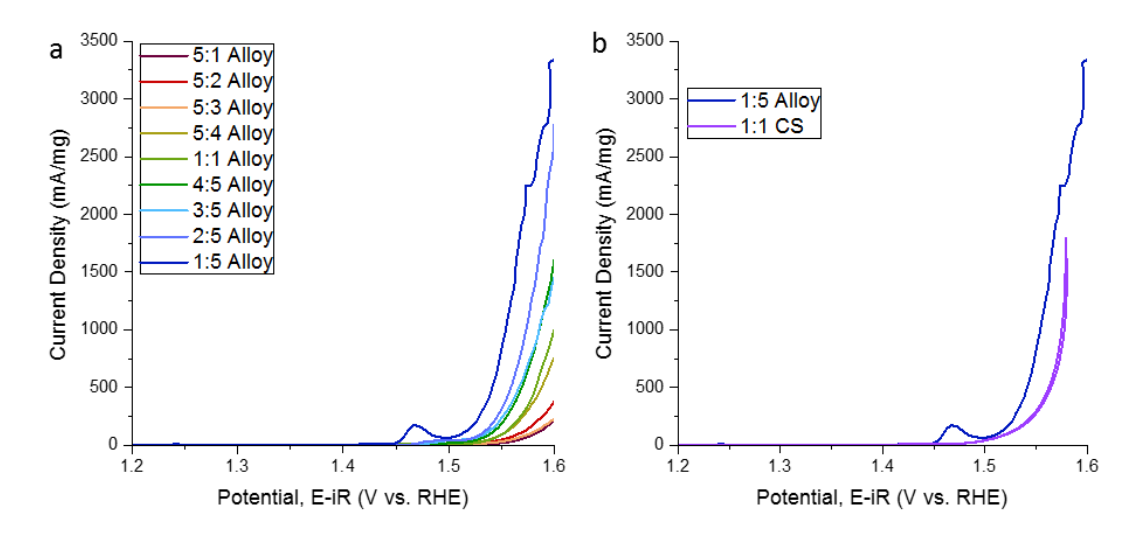


Figure 6. Nanoparticle catalyst performance on a per catalyst mass basis, where all data are reported based on the catalyst mass deposited onto a gold electrode. (a) Electrochemical performance data for alloy nanoparticles with varying Fe:Ni (mol:mol) ratio. (b) Comparison between the best-performing alloy Fe:Ni nanoparticle catalyst and the 1:1 Fe@Ni core-shell nanoparticle catalyst (32). All ratios reported are Fe:Ni (mol:mol) as synthesized.

Tafel plots of the alloy nanoparticles are shown in Figure 7. Data are summarized as a function of Fe:Ni molar ratio for similar, low PVP:Ni ratios of 0.001 - 0.002 in Figure 7a, and the effect of PVP:Ni ratio on the Tafel curve and slope is shown in Figure 7b for three sets of alloy nanoparticles (Fe:Ni ratios of 5:1, 1:1 and 1:5). A summary of the calculated Tafel slopes is shown in Figure 7c as a function of Fe:Ni ratio, where higher PVP:Ni ratios are denoted by black arrows. The summary of Tafel slopes in Figure 7c suggests several potential trends. First, there is a general reduction in the Tafel slope as the Fe:Ni ratio decreases from 5:3 to 1:5 for samples that had low PVP:Ni ratios of 0.001 -0.002. This result is not surprising as previous work on thin films has demonstrated that the performance of similar FeNi bimetallic catalysts improves as the ratio of Fe:Ni decreases from ~85% to 20% (atomic % of Fe) (11). Further, Bau et al. (22) demonstrated a similar increase in performance for a set of [Ni,Fe]O nanoparticles, as the atomic iron concentration decreased from 76% to 27%. Specifically, Bau et al. report a decrease in the measured Tafel slope from 48 mV/dec to 36 mV/dec, as the iron concentration decreased from 76% to 27% (22). In the results presented in Figure 7c, the Tafel slope similarly decreases from 54 mV/dec to 40 mV/dec with a decrease in the atomic iron concentration from 63% to 17% (i.e., for a molar Fe:Ni ratio decrease from 5:3 to 1:5).

A second trend observed in the data presented in Figure 7c is an increase in the Tafel slope for Fe:Ni ratios of 5:1 to 5:3. Further, the Tafel slope is affected by the increase in PVP:Ni ratio, where the higher ratio of 0.005 caused an increase in the Tafel slope for both molar ratios of Fe:Ni tested (1:1 and 1:5). In particular, the Tafel slope of the 1:5 Fe:Ni alloy nanoparticle catalyst increased significantly from 40 mV/dec to 64 mV/dec, with an increase in the PVP:Ni molar ratio from 0.001 to 0.005. Overall, the range of Tafel slopes calculated from the data shown in Figure 7 falls within the typical range observed for similar OER catalysts (30 – 50 mV/dec) (22), except for the result from the 1:5 Fe:Ni nanoparticles synthesized with a PVP:Ni molar ratio of 0.005. Bau et al.

suggested in their work that the Tafel slope, and therefore the OER kinetics, are strongly influenced by the available electrochemically-active surface area of the nanoparticles (22). It is possible that our results may also be affected by the available active surface area, and the trends observed in Figure 7c may be suggesting changes to the active surface area with changes in bimetallic ratio and the presence of PVP. Based on the work of Bau et al. (22), future analysis of our alloy nanoparticles will include an evaluation of the electrochemically active surface area and its importance in affecting the kinetics of OER performance. We also note that all reported Fe:Ni molar ratios in this work are based off of the theoretical ratio based on the starting concentrations of metal precursors in the synthesis solution.

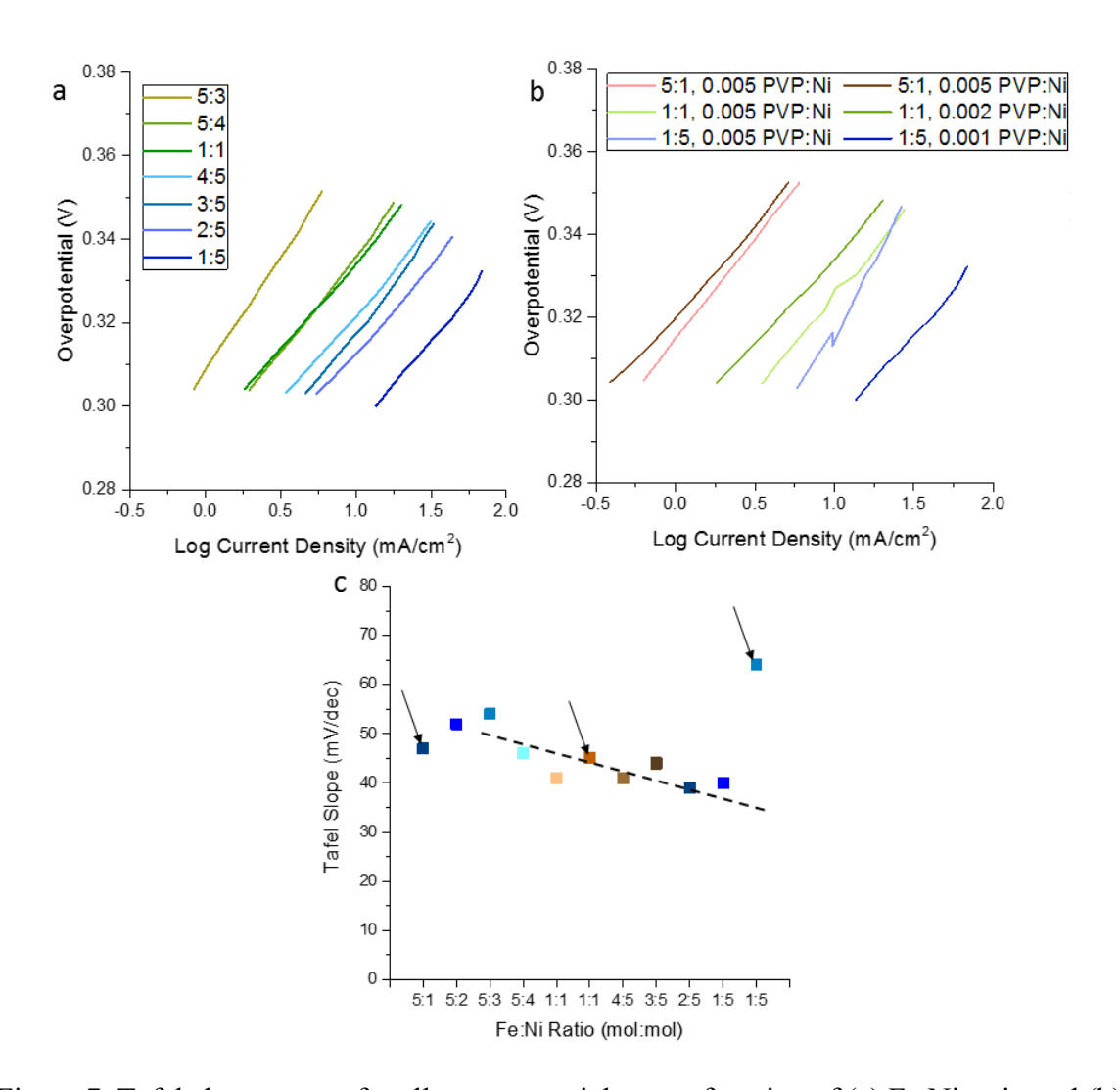


Figure 7. Tafel slope curves for alloy nanoparticles as a function of (a) Fe:Ni ratio and (b) PVP:Ni ratio. In (a), all nanoparticles had a PVP:Ni ratio of 0.001-0.002. (c) Summary of the effects of Fe:Ni ratio and PVP:Ni ratio on alloy nanoparticle catalyst performance. Arrows denote nanoparticles with the higher ratio of 0.005 PVP:Ni for the Fe:Ni ratios of 5:1, 1:1 and 1:5.

The electrochemical performance of the suite of alloy bimetallic Fe:Ni nanoparticles tested in this work is summarized in Table 1. The data for this suite of catalysts suggest that controlling the ratio of iron to nickel in the catalyst is critical to the optimization of

catalyst performance for OER. Further, this initial work on evaluating the role of PVP concentration on electrocatalytic performance suggests that PVP may also play an important role for OER performance, and the effects of PVP concentration, Fe:Ni molar ratio, and other nanoparticle characteristics (e.g., size, electrochemically active surface area) must be delineated.

TABLE I. Summary of alloy bimetallic FeNi nanoparticle electrochemical performance metrics.

Alloy Nanoparticle Fe:Ni Ratio (mol:mol)	PVP:Ni Ratio (mol:mol)	Tafel Slope (mV/dec)	Overpotential @ 10 mA/cm ² (mV)	Current Density @ 1.6 V (mA/mg catalyst)
5:1	0.005	47*	368	225
5:2	0.003	52	355	393
5:3	0.002	54	366	256
5:4	0.002	46	335	786
1:1	0.005	45	327	1353
1:1	0.002	41	334	1070
4:5	0.002	41	321	1699
3:5	0.001	44	317	1475
2:5	0.001	39	312	2894
1:5	0.005	64	313	999
1:5	0.001	40	295	3343
_	0.001 Ilues, standard deviati		295	3343

Conclusions

In this study, alloy bimetallic FeNi (Fe_xNi_y(OH)₂) nanoparticles were synthesized via an aqueous-based solution phase approach. The synthesis method can be used to produce either FeNi alloy or Fe@Ni core-shell nanoparticles. All nanoparticles synthesized had a spherical shape, and initial TEM/EDX analysis suggests that the nanoparticles contained a significant oxygen content. Alloy nanoparticles with a Fe:Ni range of 5:1 to 1:5 (mol:mol) were synthesized and evaluated for electrochemical performance as OER catalysts in alkaline electrolyte. In addition, the effect of PVP stabilizer on nanoparticle catalytic performance was evaluated for a PVP:Ni molar ratio range of 0.001 - 0.005. Electrochemical analysis suggests that the molar ratio of Fe:Ni in the alloy nanoparticles plays a critical role in the OER performance, with an increase in performance observed with a decrease in the iron content from 67% to 17% (i.e., for a Fe:Ni ratio range of 5:1 to 1:5). Alloy nanoparticles with a 1:5 ratio of Fe:Ni and a PVP:Ni ratio of 0.001 resulted in an overpotential of 295 mV at 10 mA/cm², a Tafel slope of 40 mV/dec, and a mass-based activity of 3343 mA/mg at 1.6 V vs. RHE. Experiments performed for several nanoparticle samples with varying PVP:Ni ratios suggest that the PVP concentration may play a role in catalyst performance, but further experiments are necessary to completely delineate the role of PVP in FeNi nanoparticle catalyst performance for OER.

Acknowledgments

The authors acknowledge A. Curtin of the National Institute of Standards and Technology for obtaining some of the TEM/EDX images presented in this paper. The authors acknowledge M. Benamara of the University of Arkansas Institute for Nanoscience and Engineering and the associated nanocharacterization facility for help with TEM imaging. The authors also acknowledge E.B. Coughlin of the University of Massachusetts, Amherst, for samples of experimental ionomers used in electrochemistry experiments.

References

- 1. M. S. Burke, L. J. Enman, A. S. Batchellor, S. H. Zou and S. W. Boettcher, *Chem. Mater.*, **27**, 7549 (2015).
- 2. M. S. Burke, S. H. Zou, L. J. Enman, J. E. Kellon, C. A. Gabor, E. Pledger and S. W. Boettcher, *J. Phys. Chem. Lett.*, **6**, 3737 (2015).
- 3. T. W. Capehart, D. A. Corrigan, R. S. Conell, K. I. Pandya and R. W. Hoffman, *Appl. Phys. Lett.*, **58**, 865 (1991).
- 4. D. Chen and S. D. Minteer, *J. Power Sourc.*, **284**, 27 (2015).
- 5. M. Gao, W. Sheng, Z. Zhuang, Q. Fang, S. Gu, J. Jiang and Y. Yan, *J. Am. Chem. Soc.*, **136**, 7077 (2014).
- 6. Y. Gao, H. Li and G. Yang, *Cryst. Growth Des.*, **15**, 4475 (2015).
- 7. R. S. McEwen, J. Phys. Chem., **75**, 1782 (1971).
- 8. A. Van der Ven, D. Morgan, Y. S. Meng and G. Ceder, *J. Electrochem. Soc.*, **153**, A210 (2006).
- 9. M. Wehrens-Dijksma and P. H. L. Notten, *Electrochim. Acta*, **51**, 3609 (2006).
- 10. O. Diaz-Morales, D. Ferrus-Suspedra and M. T. M. Koper, *Chem. Sci.*, 7, 2639 (2016).
- 11. D. Friebel, M. W. Louie, M. Bajdich, K. E. Sanwald, Y. Cai, A. M. Wise, M.-J. Cheng, D. Sokaras, T.-C. Weng, R. Alonso, R. C. Davis, J. R. Bargar, J. K. Norskov, A. Nilsson and A. T. Bell, *J. Am. Chem. Soc.*, **137**, 1305 (2015).
- 12. L. Trotochaud, S. L. Young, J. K. Ranney and S. W. Boettcher, *J. Am. Chem. Soc.*, **136**, 6744 (2014).
- 13. S. Klaus, Y. Cai, M. W. Louie, L. Trotochaud and A. T. Bell, *J. Phys. Chem. C*, **119**, 7243 (2015).
- 14. S. Klaus, M. W. Louie, L. Trotochaud and A. T. Bell, *J. Phys. Chem. C*, **119**, 18303 (2015).
- 15. S. Klaus, L. Trotochaud, M.-J. Cheng, M. Head-Gordon and A. T. Bell, *ChemElectroChem*, **3**, 66 (2016).
- 16. M. K. Bates, Q. Jia, H. Doan, W. Liang and S. Mukerjee, *ACS Catal.*, **6**, 155 (2016).
- 17. H. S. Ahn and A. J. Bard, *J. Am. Chem. Soc.*, **138**, 313 (2016).
- 18. H. Ali-Löytty, M. W. Louie, M. R. Singh, L. Li, H. G. Sanchez Casalongue, H. Ogasawara, E. J. Crumlin, Z. Liu, A. T. Bell, A. Nilsson and D. Friebel, *J. Phys. Chem. C*, **120**, 2247 (2016).
- 19. M. W. Louie and A. T. Bell, *J. Am. Chem. Soc.*, **135**, 12329 (2013).
- 20. A. G. El-Deen, M. El-Newehy, C. S. Kim and N. A. Barakat, *Nanoscale Res. Lett.*, **10**, 104 (2015).
- 21. K. Fominykh, P. Chernev, I. Zaharieva, J. Sicklinger, G. Stefanic, M. Döblinger, A. Müller, A. Pokharel, S. Böcklein, C. Scheu, T. Bein and D. Fattakhova-Rohlfing, *ACS Nano*, **9**, 5180 (2015).
- 22. J. A. Bau, E. J. Luber and J. M. Buriak, ACS Appl. Mater. Inter., 7, 19755 (2015).
- 23. Y. Q. Gao, X. Y. Liu and G. W. Yang, *Nanoscale*, **8**, 5015 (2016).
- 24. W. Ma, R. Ma, C. Wang, J. Liang, X. Liu, K. Zhou and T. Sasaki, *ACS Nano*, **9**, 1977 (2015).
- 25. Y. Qiu, L. Xin and W. Li, *Langmuir*, **30**, 7893 (2014).
- 26. D. Tang, J. Liu, X. Wu, R. Liu, X. Han, Y. Han, H. Huang, Y. Liu and Z. Kang, *ACS Appl. Mater. Inter.*, **6**, 7918 (2014).
- 27. Y. Lu, Y. Wang and W. Chen, *J. Power Sourc.*, **196**, 3033 (2011).

- 28. N. V. Long, M. Ohtaki, M. Nogami and T. D. Hien, *Coll. Polym. Sci.*, **289**, 1373 (2011).
- 29. C. Susut, D.-J. Chen, S.-G. Sun and Y. J. Tong, *Phys. Chem. Chem. Phys.*, **13**, 7467 (2011).
- 30. L. F. Greenlee and S. A. Hooker, *Desalin. Water Treat.*, 37, 114 (2012).
- 31. L. F. Greenlee and N. S. Rentz, *J. Nanopart. Res.*, **16**, 2712 (2014).
- 32. S. L. Candelaria, N. M. Bedford, T. J. Woehl, N. S. Rentz, A. R. Showalter, S. Pylypenko, B. A. Bunker, S. Lee, B. Reinhard, Y. Ren, S. P. Ertem, E. B. Coughlin, N. A. Sather, J. L. Horan, A. M. Herring and L. F. Greenlee, *ACS Catal.*, 7, 365 (2017).